

# Shunt Characterization Technique of Decoupling Transmission Line for Millimeter-Wave CMOS Amplifier Design

Korkut Kaan Tokgoz, Kimsrun Lim, Kenichi Okada, and Akira Matsuzawa

Tokyo Institute of Technology, Department of Physical Electronics, 2-12-1-S3-27, Oookayama, Meguro-ku, Tokyo, 152-8552, Japan, E-mail:korkut@ssc.pe.titech.ac.jp

**Abstract** — A shunt characterization method is proposed to characterize a very low impedance transmission line (TL), which is used for decoupling of DC and RF in millimeter-wave CMOS circuits. Since metal-insulator-metal (MIM) capacitors are used to achieve very low impedance the TL named as MIM TL. Two structures are used for this method. S-parameters of MIM TL are calculated using reflections. The results match better than direct measurement method from 1 to 110 GHz.

**Index Terms** — CMOS, decoupling, device characterization, metal-insulator-metal, mm-wave, transmission line.

## I. INTRODUCTION

CMOS millimeter-wave research still preserves its importance due to capabilities of several Gb/s high-data-rate communications, low cost, and monolithic implementation with analog and digital circuitry [1]-[3]. A successful implementation of such a high-data-rate transceiver, first of all, requires accurate active and passive device models. Process design kits (PDKs) from foundries have very accurate models up to around 20 GHz. Thus for low frequency analog circuits and digital circuits PDK models can be used. Unfortunately, this is not the case for millimeter-wave circuits. For this frequency region, the active and passive components to be used in the system have to be characterized and modeled beforehand of the circuit design phase. Hence characterization of devices is the first important step for millimeter-wave circuit design. To provide an example, Fig. 1 illustrates a simple common-source amplifier. One can observe the input and output matching blocks of this amplifier. In general, for millimeter-wave amplifiers these blocks include transmission lines (TLs), tee-junctions, and bends. DC cut capacitors and bias resistors are used for transistor biasing. A common way to decouple DC and RF is to use lumped-constant components like inductors and capacitors. However, at these high frequencies these components on silicon cannot be considered as lumped anymore. Hence the simulation accuracy decreases considerable, which affects the overall performance of the circuits. Instead of lumped-constant components, a TL with very low characteristic impedance (around 1-3 $\Omega$ ) can be used, assuring the design accuracy [1]-[3]. In order to decrease the characteristic impedance for this decoupling TL, metal-insulator-metal (MIM) capacitors are used in this structure, and for that reason this TL is referred as MIM TL and can be observed in Fig. 1. There are several advantages of MIM TL.

First of all, it can be characterized as per-unit-length like a normal TL and hence scalable. Moreover, MIM TL decreases the effects caused by DC feed networks unknown responses at millimeter-wave frequencies. However, the characterization of this structure is a hard task owing to its very low characteristic impedance when measured in a 50 $\Omega$  system [4]. In this paper, for the above presented reasons, a shunt characterization method is presented for MIM TL.

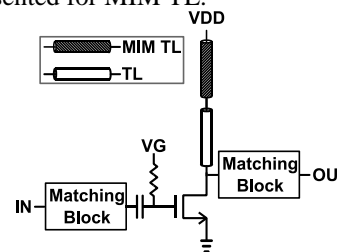


Fig. 1. Representation of a simple common-source amplifier with input and output matching blocks, DC cut capacitor, bias resistor, TL, and MIM TL used for decoupling of RF and DC.

## II. MIM TL AND CHARACTERIZATION STRUCTURES

Fig. 2 illustrates metal layers of MIM TL, briefly. The top metal layer width is adjusted to 12  $\mu\text{m}$  (in a normal TL the width is 2.5  $\mu\text{m}$  to have around 50 $\Omega$  characteristic impedance) to decrease the inductive component of TL. To increase the capacitive component of the TL, several methods are used; such as, the space between the signal line and grounds adjusted to 2.5  $\mu\text{m}$ , the metal layer below top metal adjusted such that parallel plate capacitances are formed (gray areas in Fig. 2), and MIM capacitors are included below this metal layer (blue areas seen in the cross-sectional view). Additionally, 4 metal layers are adjusted below this parallel plate capacitance with many finger capacitances and connected with each other using vias and connected to signal line (below the red circle in Fig. 2). With these methods the characteristic impedance of MIM TL decreased as low as around 1-3 $\Omega$ . However, as mentioned above, this structure is hard to characterize using direct measurements (Fig. 3(c)) considering accuracy. For that reason, two characterization structures are proposed as in Fig. 3(a), (b). The MIM TLs are connected in shunt configuration in these two structures. In both structures symmetric parts of the tee-junctions are connected to probing pads with 40  $\mu\text{m}$  TLs. In Fig. 3(a), third

port of tee-junction is terminated with a 10  $\mu\text{m}$  TL followed with a 40  $\mu\text{m}$  MIM TL. The other end of the MIM TL left open circuited. In the other characterization structure (Fig. 3(b)), third port of tee-junction is terminated with two repeated structures of the first one. These two structures are used for characterization of MIM TL, and described in detail in the next section.

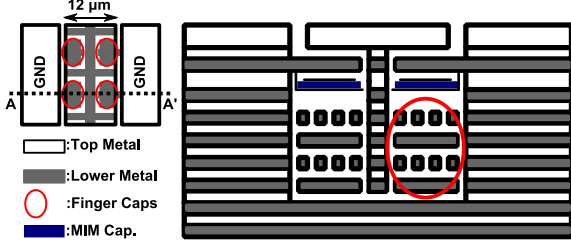


Fig. 2. Illustration of metal layers for MIM TL

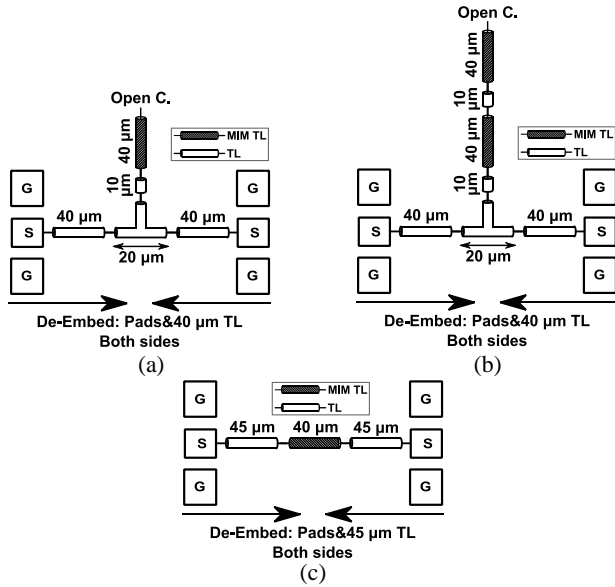


Fig. 3. Shunt characterization structures for MIM TL (a) one 40  $\mu\text{m}$  MIM TL shunt connected, (b) two 40  $\mu\text{m}$  MIM TL shunt connected with 10  $\mu\text{m}$  normal TL interconnected, and (c) conventional characterization structure.

### III. METHOD AND MEASUREMENT RESULTS

The first step of characterization is the de-embedding of the probing pads and 40  $\mu\text{m}$  TLs connected between pads and tee-junctions for the two structures from both sides. The de-embedding method used for this work is L-2L method owing to its accuracy [5], [6]. In [6], different de-embedding methods are used to characterize the pads, TLs, and other elements, and their effects are observed on a 4-stage power amplifier. According to results the L-2L de-embedding method gives the most accurate results. Same method is used to characterize the pads and TLs. Thus, pads and 40  $\mu\text{m}$  TLs are de-embedded from both sides of structures (Fig. 3(a), (b)). The remaining structures are provided in Fig. 4(a) and (b), respectively. MIM TL is assumed to be symmetrical and reciprocal as presented

in (1). To characterize MIM TL one can find the S-parameters with the following method. The common structure in Fig. 4(a) and (b) is 10  $\mu\text{m}$  TL connected to the third port of tee-junction as can be observed in Fig. 5. Note that tee-junction is characterized beforehand up to 110 GHz. This overall structure presented in Fig. 5 has an S-parameter response as presented in (2). Note that the structure is symmetric for ports 1 and 2. All parameters in this structure are known beforehand. When this three port structure is terminated with a device having reflection coefficient of  $\Gamma$ , the two port S-parameter matrix can be represented as in (3). The reflection coefficient of MIM TL when one end is open circuited can be calculated as in (4) using the terms in (1). The two port S-parameters of Fig. 4(a) is provided in (5).  $\Gamma_{\text{MIM}}$  can be calculated using (5) as given in (6). Similarly,  $\Gamma_2$  can be calculated from the results of Fig. 4(b) and presented in (7).

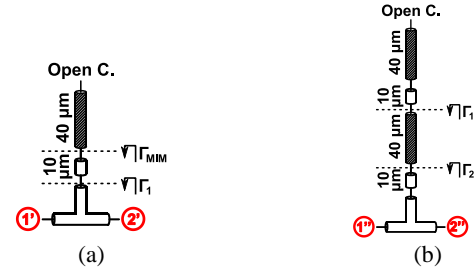


Fig. 4. De-embedded structures for MIM TL from Fig. 3(a) and (b), accordingly.

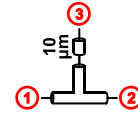


Fig. 5. Port definition of Tee-junction with 10  $\mu\text{m}$  TL connected.

$$[S_{\text{MIMTL}}] = \begin{bmatrix} S_{\text{MIMTL11}} & S_{\text{MIMTL21}} \\ S_{\text{MIMTL21}} & S_{\text{MIMTL11}} \end{bmatrix} \quad (1)$$

$$[S_{\text{T-TL}}] = \begin{bmatrix} S_{11} & S_{21} & S_{13} \\ S_{21} & S_{11} & S_{13} \\ S_{13} & S_{13} & S_{33} \end{bmatrix} \quad (2)$$

$$[S_{\text{T-TL}}^{3,\Gamma}] = \begin{bmatrix} S_{11} & S_{21} \\ S_{21} & S_{11} \end{bmatrix} + S_{13}^2 / (1/\Gamma - S_{33}) \begin{bmatrix} 1 & 1 \\ 1 & 1 \end{bmatrix} \quad (3)$$

$$\Gamma_{\text{MIM}} = S_{\text{MIMTL11}} + S_{\text{MIMTL21}}^2 / (1 - S_{\text{MIMTL11}}) \quad (4)$$

$$[S_{\text{Meas}}^{\Gamma_{\text{MIM}}}] = \begin{bmatrix} S_{11} & S_{21} \\ S_{21} & S_{11} \end{bmatrix} + S_{13}^2 / (1/\Gamma_{\text{MIM}} - S_{33}) \begin{bmatrix} 1 & 1 \\ 1 & 1 \end{bmatrix} \quad (5)$$

$$\Gamma_{\text{MIM}} = 1 / (S_{33} + S_{13}^2 / (S_{\text{Meas},11}^{\Gamma_{\text{MIM}}} - S_{11})) \quad (6)$$

$$\Gamma_2 = 1 / (S_{33} + S_{13}^2 / (S_{\text{Meas},11}^{\Gamma_2} - S_{11})) \quad (7)$$

We can also relate  $\Gamma_2$  to MIM TL S-parameters and  $\Gamma_1$  as in the following equation and can be observed in Fig. 4(b). Moreover,  $\Gamma_1$  can be found by terminating a 10  $\mu\text{m}$  TL with  $\Gamma_{\text{MIM}}$ , and this calculation is shown in (9).

$$\Gamma_2 = S_{\text{MIMTL11}} + S_{\text{MIMTL21}}^2 / (1/\Gamma_1 - S_{\text{MIMTL11}}) \quad (8)$$

$$\Gamma_1 = S_{TL-10\mu m,11} + \frac{S_{TL-10\mu m,21}^2}{(1/\Gamma_{MIM} - S_{TL-10\mu m,11})} \quad (9)$$

The only remaining steps are to calculate S-parameters of MIM TL.  $S_{MIMTL11}$  can be calculated as in (10). After  $S_{MIMTL11}$  is calculated, using (4)  $S_{MIMTL21}$  can also be calculated as presented in (11).

$$S_{MIMTL11} = \frac{(\Gamma_2 - \Gamma_{MIM}\Gamma_1)}{1 + (\Gamma_2 - \Gamma_{MIM} - 1)\Gamma_1} \quad (10)$$

$$S_{MIMTL21} = \sqrt{(\Gamma_{MIM} - S_{MIMTL11})(1 - S_{MIMTL11})} \quad (11)$$

The structures are fabricated in 65 nm standard CMOS process. The manufactured structures can be observed in Fig. 6. S-parameters of 40  $\mu m$  length MIM TL are found using the proposed method and compared with conventionally found (Fig. 3(c)) results in Fig. 7(a) and (b), respectively for return loss and insertion loss from 1 to 110 GHz. In order to verify the calculated MIM TL response, the structures in Fig. 3(a), (b) are reconstructed using models of TLs, tee-junctions, and MIM TL results of calculated with conventional and proposed method. They are compared with measurement results and presented in Fig. 8. Black lines represent measurement results, red lines represent model results with proposed method, and blue lines represent model results with conventional method. Fig. 8(a) gives the comparison of return losses of model and measurements results of the structure in Fig. 3(a), similarly Fig. 8(b) presents the insertion loss comparison of the same structure. Accordingly, Fig. 8(c) and (d) gives the return loss and insertion loss comparisons of Fig. 3(b). One can observe that the calculated model results match better than the conventional method up to 110 GHz. The difference between two cases at the end of frequency band caused from tee-junction model accuracy.



Fig. 6. Chip micrograph of Fig. 3(a) and (b).

#### IV. CONCLUSION

MIM TL, which has very low characteristic impedance, is characterized using shunt connected structures. Two structures are used for the calculation of MIM TL S-parameter response. The comparisons of proposed and conventional method, and measured structures show that proposed method has better agreement from 1 to 110 GHz with measurement results.

#### ACKNOWLEDGEMENT

This work was partially supported by MIC, SCOPE, MEXT, STARC, and VDEC in collaboration with Cadence Design Systems, Inc., and Agilent Technologies Japan, Ltd.

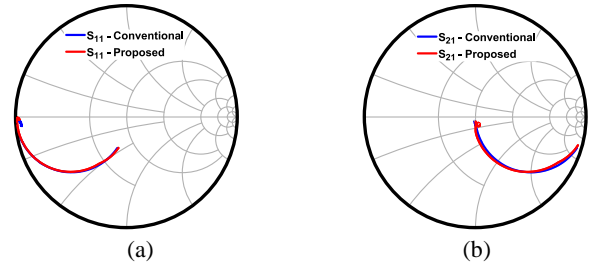


Fig. 7. Calculated S-parameter response comparison of 40  $\mu m$  MIM TL from 1 to 110 GHz with proposed method and conventional (Fig. 3(c)) method (a)  $S_{11}$ , and (b)  $S_{21}$ .

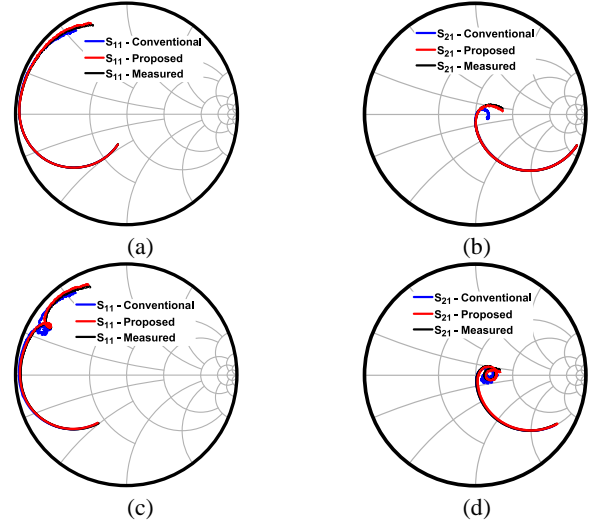


Fig. 8. Comparison between proposed model, conventional model and measurement results (black lines for measurement result, red lines for proposed model results, and blue lines for conventional model results) from 1 to 110 GHz (a)  $S_{11}$  of Fig. 3(a), (b)  $S_{21}$  of Fig. 3(a), (c)  $S_{11}$  of Fig. 3(b), and (d)  $S_{21}$  of Fig. 3(b).

#### REFERENCES

- [1] K. Okada, *et al.*, "Full Four-Channel 6.3-Gb/s 60-GHz CMOS Transceiver With Low-Power Analog and Digital Baseband Circuitry," *IEEE JSSC*, vol. 48, no. 1, pp. 46-65, Jan. 2013.
- [2] K. Okada, *et al.*, "A 60-GHz 16QAM/8PSK/QPSK/BPSK Direct-Conversion Transceiver for IEEE802.15.3c," *IEEE JSSC*, vol. 46, no. 12, pp. 2988-3004, Dec. 2011.
- [3] Y. Natsukari, and M. Fujishima, "36 mW 63 GHz CMOS Differential Low-Noise with 14 GHz Bandwidth," *Symp. VLSI Circuits Dig. Tech. Papers*, Jun. 2009, pp. 252-253.
- [4] S. Maki, S. Kawai, K. Okada, and A. Matsuzawa, "A Millimeter-Wave Shunt Measurement Technique for Low-Impedance Elements," *IEICE Society Conf.*, C-12-17, Sep. 2013 (in Japanese).
- [5] N. Li, K. Matsushita, N. Takayama, S. Ito, K. Okada, and A. Matsuzawa, "Evaluation of a Multi-Line De-embedding Technique up to 110 GHz for Millimeter-Wave CMOS Circuit Design," *IEICE Trans. Fundam. Electron.*, vol. E93-A, no. 2, pp. 431-439, Feb. 2010.
- [6] R. Minami, C. Han, K. Matsushita, K. Okada, and A. Matsuzawa, "Effect of Transmission Line Modeling Using Different De-embedding Methods," *EuMC*, Oct. 2011, pp. 381-384.